NASA TECHNICAL NOTE

NASA TN D-5680

c. 1

NASA TN D-5680

METEOROLOGICAL SATELLITE VIEWS OF CLOUD GROWTH ASSOCIATED WITH THE DEVELOPMENT OF SECONDARY CYCLONES

by William E. Shenk

Goddard Space Flight Center
Greenbelt, Md.

NATIONAL AERONAUTICS AND SPACE ADMINISTRATION • WASHINGTON, D. C. • APRIL 1970

1. Report No.	2. Government Accession No.	3. Recipient's Catalog No.
NASA TN D-5680		

4. Title and Subtitle
Meteorological Satellite Views of Cloud Growth Associated with the Development of Secondary Cyclones

5. Report Date
April 1970

6. Performing Organization Code

7. Author(s)
William E. Shenk

8. Performing Organization Report No.
G-966

9. Performing Organization Name and Address
Goddard Space Flight Center
Greenbelt, Maryland 20771

10. Work Unit No.
160-44-03-02-51

11. Contract or Grant No.

12. Sponsoring Agency Name and Address
National Aeronautics and Space Administration
Washington, D. C. 20546

13. Type of Report and Period Covered
Technical Note

14. Sponsoring Agency Code

15. Supplementary Notes

16. Abstract

During March 1962 the cloud changes associated with the pre-development and development periods of two secondary cyclones in the North Pacific Ocean were viewed on at least two successive days by the 8-12μ "window" channel of the TIROS IV meteorological satellite. Both secondary cyclones developed at the base of the occlusion. For the two cases, when the secondary circulations were first noticeable on the surface chart, the equivalent blackbody temperatures (T_{BB}) as measured by the radiometer averaged 15°K colder than the day before in the northeast quadrant relative to the base of the occlusion. The average T_{BB} was taken over an area of approximately 300,000 square miles. For two other cases, an average warming of 4°K occurred from day to day over the same area relative to the base of the occlusion when no significant secondary development occurred and when the primary occluded cyclone was slowly weakening. These results suggest that, with the assistance of meteorological satellite radiation data, considerable cloud growth is noticeable prior to the generation of a secondary cyclone at the base of the occlusion.

17. Key Words Suggested by Author	18. Distribution Statement
TIROS IV Secondary Cyclone Equivalent Blackbody Temperature Occlusion	Unclassified—Unlimited

19. Security Classif. (of this report)	20. Security Classif. (of this page)	21. No. of Pages	22. Price*
Unclassified	Unclassified	26	$3.00

*For sale by the Clearinghouse for Federal Scientific and Technical Information
Springfield, Virginia 32151

CONTENTS

METEOROLOGICAL SATELLITE VIEWS OF CLOUD GROWTH ASSOCIATED WITH THE DEVELOPMENT OF SECONDARY CYCLONES

by
William E. Shenk
Goddard Space Flight Center

INTRODUCTION

A secondary extratropical cyclone is a cyclone which forms near, or in association with, a primary cyclone. Often the secondary cyclone intensifies and deepens sufficiently to absorb the circulation of the primary cyclone, thus becoming the only remaining circulation. There seem to be two preferred areas of development relative to the primary cyclone: one area at the base of the occlusion, the other southwest of the base of the occlusion along the trailing cold front. From either of these preferred locations, development often proceeds rapidly. Thus, it is important that the presence of these new circulations be determined quickly. Early detection is especially difficult over oceans, where conventional meteorological data are sparse.

The East Coast of the United States is a preferred area for secondary development. This usually occurs along (or just off) the coastline, during the late fall, winter, and early spring period, from the Carolinas to New Jersey while the primary cyclone is advancing through the Great Lakes. Early warning of the secondary development is often provided by rapidly falling barometric pressures east of the Appalachian Mountains, and swift advance of the precipitation shield and/or intensification of precipitation over the same region. The behavior of the precipitation patterns suggests that changes might be noted in the cloud deck that would indicate secondary development at an earlier stage. Substantial changes in the areal extent and/or vertical development of clouds near the region of secondary development would be anticipated prior to, or coincident with, the evidence of a surface circulation. Cloud changes noted during the early stages of United States East Coast secondary developments are assumed to be similar for secondary developments over oceanic areas. Over land areas, where conventional meteorological data are plentiful (such as the United States East Coast), surface observations provide information on the clouds from below. Meteorological satellites can provide cloudiness information from above, while cloud base and cloud top heights can frequently be calculated from radiosonde measurements. Additional such information is supplied by the numerous aircraft flying in the eastern half of the United States. Over the oceans, the only sensors capable of providing detailed cloud information over large areas are carried on board meteorological satellites. The purpose of this

paper is to determine what three-dimensional cloud changes occur with the development of secondary cyclones over oceanic regions as seen by meteorological satellites.

Background

Past research has shown that striking cloud formations observed by satellites are indicative of the presence of a secondary cyclone. Using the vidicon data from TIROS IX, Anderson et al. (1966) showed evidence of a secondary development in the Pacific by noting two cyclonic cloud spirals that were close together. One spiral was associated with an old occluded cyclone and the other with a new wave that had developed on a front to the southeast of the occluded storm. The double cloud spiral is anomalous to the classic cloud pattern associated with a simple occluded system (Boucher, et al., 1963).

Another case of secondary storm development as seen by a satellite has been documented by Sherr and Rogers (1965). This system was spawned along the trailing cold front some 14° south of the old occluded primary cyclone. A pronounced widening of the frontal cloud band was noticeable both in the TIROS IV vidicon pictures and in the patterns of equivalent blackbody temperatures from the window radiation channel of a five-channel scanning medium resolution radiometer carried on board the same satellite. The window radiation measurements also showed that a sizable area of relatively low equivalent blackbody temperatures indicating relatively high cloud tops was located just west and north of the surface position of the secondary cyclone, and this area was detached from the higher clouds further north near the primary storm center. This particular secondary cyclone, which was only a weak wave when the pronounced bulging was observed, intensified rapidly and became the main storm within twenty-four hours.

The above discussion indicates that by the time a surface secondary wave has developed along a trailing cold front, substantial three-dimensional cloud growth has occurred along the frontal cloud band. It is still not clear when this cloud growth commences relative to the time when the secondary cyclone can be detected by conventional data. The substantial three-dimensional cloud growth noted by Sherr and Rogers (1965) in the development of the Pacific secondary cyclone suggests that large changes in the clouds may precede secondary surface development.

Case Selection

In order to study the three-dimensional cloud changes associated with secondary storm development, radiation data are needed over a substantial portion of the eastern semicircle of the primary storm circulation for at least two consecutive days. A suitable period that met the above criteria encompassed selected dates in March, 1962 when two secondaries developed near the base of the occlusion which extended south and east of the primary cyclone center in the North Pacific Ocean. The window radiation data were provided by the five-channel medium resolution radiometer on board the TIROS IV meteorological satellite. Also, two cases were selected during the same month and year when little or no secondary development was noticeable. The cloud changes were observed during the gradual weakening process of the occlusion associated with the primary cyclone and compared with the cloud changes noted with secondary development.

Table 1 is a summary of the dates, times, and orbit numbers for each case. The satellite coverage was at night; thus, there were no concurrent vidicon data.

TIROS IV Satellite

The TIROS IV meteorological satellite was injected into an orbit with an apogee of 845 km, perigee of 710 km, period of 100.4 minutes, and inclination of 48.30 degrees. Other detailed information on the spacecraft can be found in the TIROS IV Radiation Data Catalog and Users' Manual (1963).

Table 1

Summary of TIROS IV Radiation Data Used for Each Case.

Case Number	Date	Time (GMT) (Approximate)	Orbit Number
1	March 3, 1962	1200	329, 330
	March 4, 1962	1200	344, 345
	March 5, 1962	1100	358, 359
2	March 16, 1962	1000	514, 515, 516
	March 17, 1962	0900	528, 529, 530
3	March 19, 1962	1000	558
	March 20, 1962	0900	572
	March 21, 1962	0900	586
4	March 21, 1962	0700	585
	March 22, 1962	0400	598

THE FIVE-CHANNEL SCANNING MEDIUM RESOLUTION RADIOMETER EXPERIMENT

The TIROS IV five channel medium resolution scanning radiometer was mounted in the satellite such that the optical axes were inclined 45° to the satellite spin axis. The viewing directions were designated as "floor" or "wall" according to their orientation in the satellite. Two of the channels responded to emitted terrestrial radiation from the earth and its atmosphere, two more channels sensed reflected solar radiation and the fifth channel was used to transmit a redundant time reference signal. At a satellite altitude of about 780 km, the resolution of the radiometer is about 68 km at nadir.

One channel sensed terrestrial radiation in the 8-12μ atmospheric window. The upwelling radiation was received in this spectral region primarily from the earth's surface and/or clouds. A minor contribution to the total sensed radiance comes from atmospheric constituents—principally water vapor and ozone. Since this study is concerned with radiance changes from day to day, precise knowledge of the absolute measurement is not necessary. Therefore, the ozone and water vapor contributions to the total radiance were ignored.

Following the launch of TIROS IV, some degradation of the radiometer occurred. Figure 1 is a nomogram reproduced from the TIROS IV Radiation Data Catalog and User's Manual and depicts the corrections to be added to the measurements as a function of equivalent blackbody temperature and orbit number. The corrections were derived from monitoring the quasi-global emitted radiant power during the lifetime of the satellite. As seen from Table 1, the orbits used in this study embrace the period when the degradation corrections were still changing. However, at a scene temperature of 240°K, the change in the correction over the period of study (orbits 329 to 598) was less than 1K. Thus, the changes in equivalent blackbody temperature from day to day were caused by real differences in emitted radiation rather than swift degradation of the radiometer. Therefore, since only radiance changes are considered to be important, no corrections were made for the degradation of the radiometer.

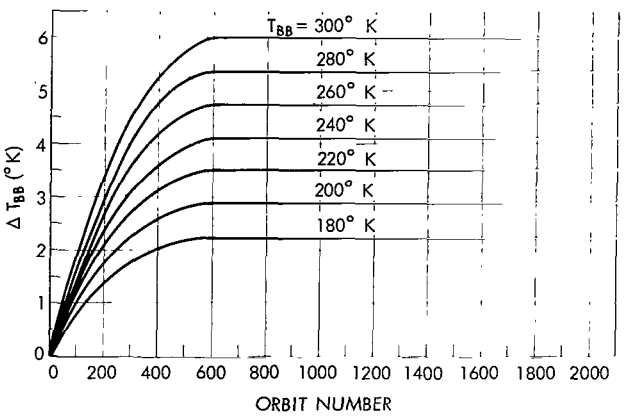

Figure 1—Equivalent blackbody temperature corrections (ΔT_{BB}) to be added to the TIROS IV window radiation wall or floor measurements of equivalent blackbody temperature as a function of orbit number.

A convenient method of displaying the radiometric data is on a grid print map. At each grid point the digitized equivalent blackbody temperatures closest to the geographical location of the grid point are averaged and this average is printed. A Mercator map projection with a 1: 10,000,000 map scale was used in this study. The spacing of the grid points (called the mesh interval) was 1.25° of longitude for this scale. Near the nadir, about five digitized scan spots were averaged per grid point.

There are errors in the geographical positioning of the radiation data. These errors (approximately 1° of latitude) are a combination of uncertainties both in the scan nadir angle and in the attitude of the spin axis. In view of the synoptic scale of this investigation, an error of about one mesh interval was not considered serious enough to make an attempt to locate the data more accurately.

There are three possible earth scanning modes of the TIROS radiometers (Bandeen, 1962). Figure 2 depicts these modes, which can be described as follows:

1. Closed Mode — All of the scan spots for a number of spin cycles were earth viewed, either through the "wall" or "floor" sensor.

2. Single Open Mode — The scan spots of a spin cycle are divided between earth viewed and space viewed through the "wall" sensor only or through the "floor" sensor only.

3. Alternating Open Mode — The scan spots from a given spin cycle are a combination of space and earth viewed, alternately through the "wall" and "floor" sensors.

Radiation data acquired when the satellite was viewing in the closed mode are not usable as the probability is high that these data are located inaccurately. The most reliable data were gathered from the single open mode swaths and wherever possible, these data were used. In order to provide the desired 24-hour continuity over a substantial portion of a cyclone, use of some alternating open mode data was necessary.

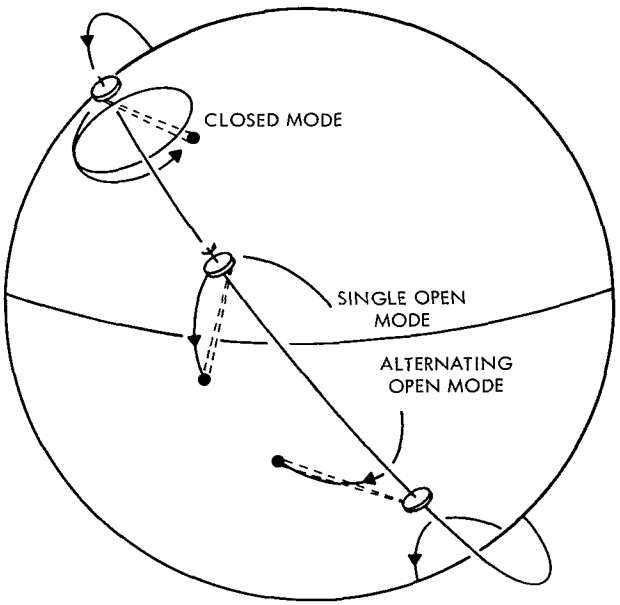

Figure 2—The three scanning modes of the TIROS radiometers.

Occasionally, there are errors in properly locating the alternating open mode data. These are caused by incorrect identification of whether a particular swath was from the "wall" or the "floor" sensor. Since one of the viewing directions is looking well forward of the subsatellite point and the other well behind, substantial location errors can result. A listing of each digitized sample for each swath shows whether the interlace of floor and wall swaths is erratic. The listings were checked for the orbits where only alternating open mode data were used and the data discarded if they appeared to be improperly located. For cases where the alternating open mode coverage was a small portion of the total coverage, concurrent single open mode data were examined to see if the data fields matched each other for the portion of the map where the dual coverage existed. A final test of reasonable data location was the position of the radiation data relative to the locations of weather features. No serious discrepancies were noted.

SUMMARY OF THE CASES

Grid print maps of the window radiation data were prepared at approximately 24-hour intervals. Individual maps were prepared for each orbit instead of compositing the data for a series of orbits on one map when it became necessary to use data from more than one orbit for maximum coverage of a cyclone. The data along the edges of orbits adjacent to the one which gave the primary coverage of a cyclone were then shifted slightly to fit the data along the edges of the primary coverage orbit. Movement of the clouds in one TIROS orbital period probably causes most of the shift in the radiation patterns (some of the shift could be caused by attitude differences between orbits).

Figures 3-5 depict the window radiation patterns for March 3, 4, and 5, respectively. In these and all of the remaining figures showing radiation measurements, the dashed lines indicate radiation data spliced from orbits adjacent to the primary coverage orbit. Frontal positions were determined from synoptic charts prepared by the National Meteorological Center (NMC).

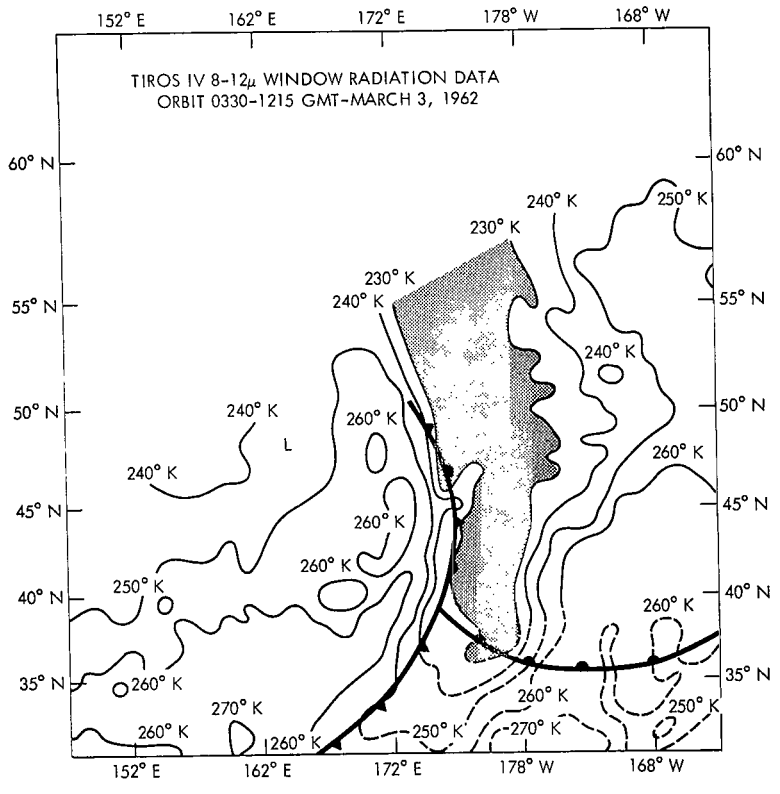

Figure 3—TIROS IV window radiation data for March 3, 1962 (orbit 330). Dashed lines show data added from orbit 329.

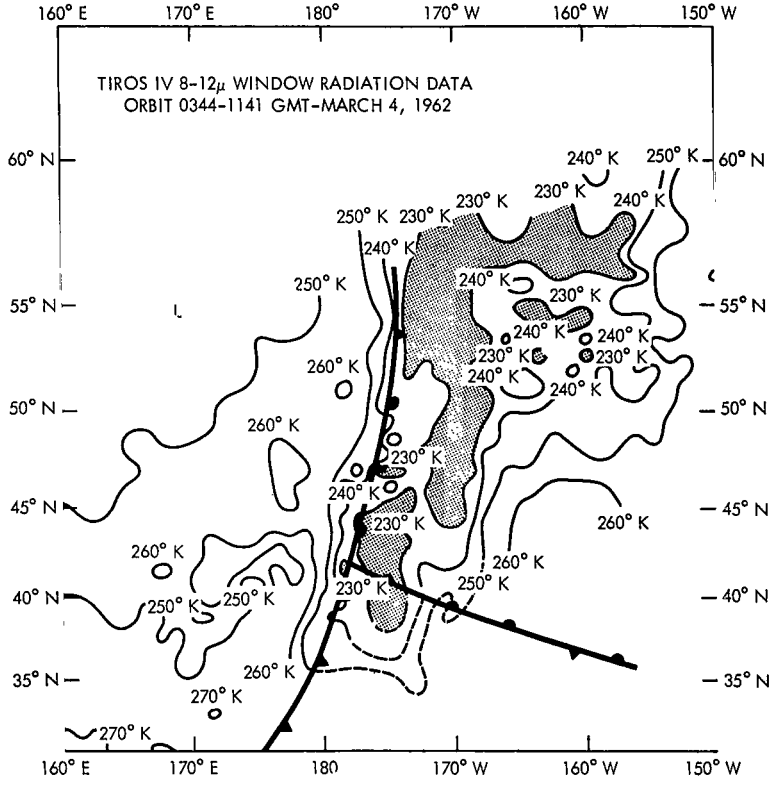

Figure 4—TIROS IV window radiation data for March 4, 1962 (orbit 344). Dashed lines show data added from orbit 343.

Some adjustment was occasionally made in the frontal position to fit the cloud patterns, without violating conventional surface observations. The eastern Pacific case was one where a very weak wave developed on the front to the south-southeast of the primary cyclone. This wave, shown as a dashed L in Figure 5, rippled rapidly up the front as a stable wave and filled within 24 hours. There was never evidence of a complete circulation on any surface map during the short history of the system. Gradual weakening of the occlusion occurred during the three-day period and is reflected in the changes in the radiation field. The coverage of equivalent blackbody temperatures below 230°K was quite extensive on March 3 and only spotty on March 5 while the size of the frontal band changed little. Figures 6-8 show the surface charts for 1200 GMT for the same three days. These figures illustrate the steady weakening and filling of the large primary cyclone and the position and strength of the minor wave mentioned above. A 500 mb broad trough was present in the region for the same period. On the last day (March 5) the 500 mb broad stream was perturbed by a weak short wave trough which probably contributed to the formation of the weak wave at 42°N, 170°W (Figure 8).

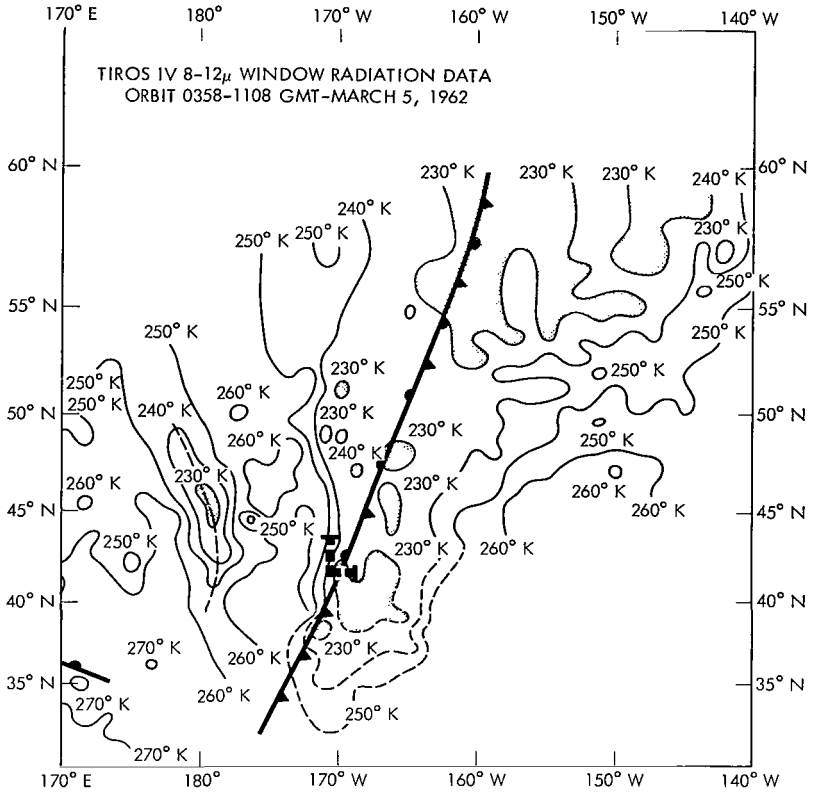

Figure 5—TIROS IV window radiation data for March 5, 1962 (orbit 358). Dashed lines show data added from orbit 357.

The window radiation patterns and surface analyses are presented in Figures 9-12 for the remaining case where no secondary cyclone development occurred near the base of the occlusion. The trend of increased equivalent blackbody temperatures was also noted in this case in the region immediately to the east and northeast of the base of the occlusion, reflecting the gradual weakening of the frontal band. A large area of equivalent blackbody temperatures of $\leq$ 230°K was located some 300 nautical miles east of the base of the occlusion at 1000 GMT, March 16 (Figure 9). This area had disappeared relative to the base of the occlusion 23 hours later (Figure 10). The large

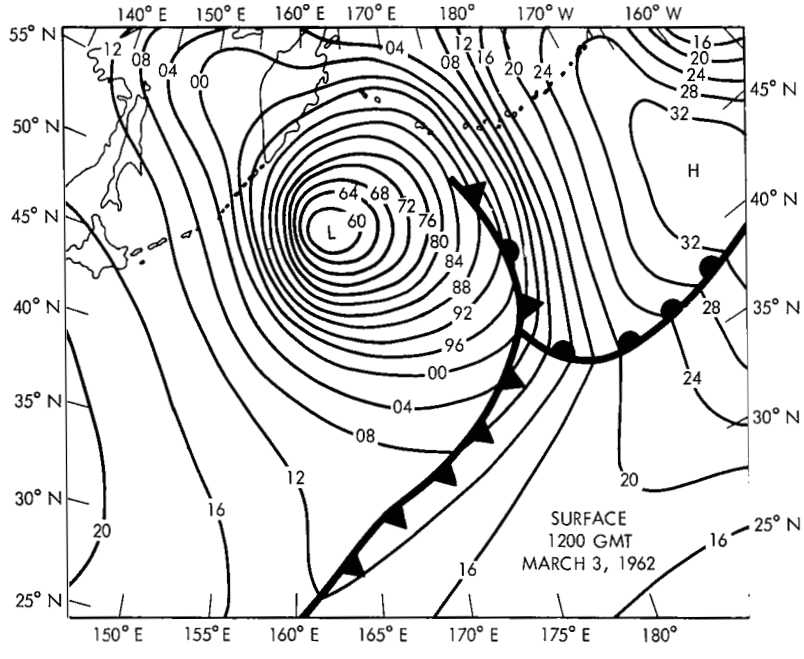

Figure 6—Surface chart for 1200 GMT, March 3, 1962.

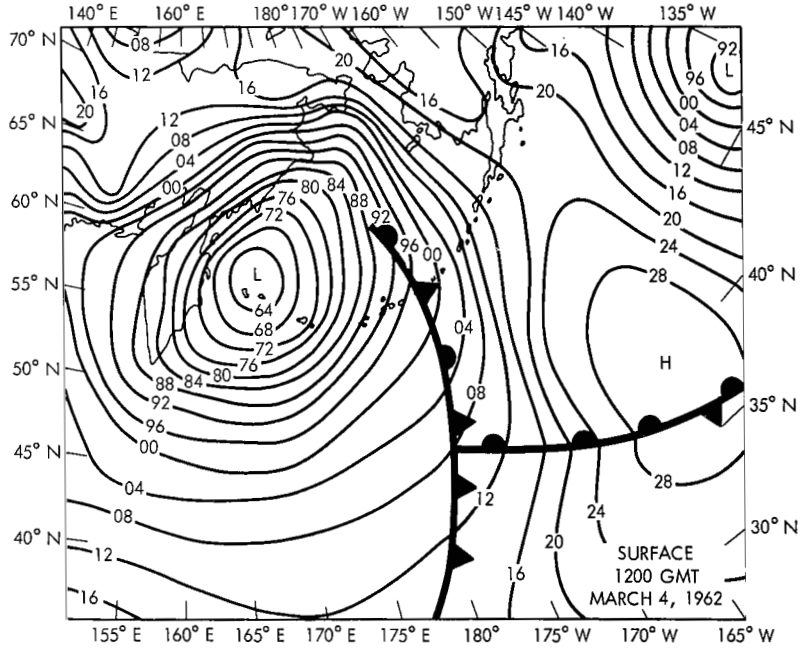

Figure 7—Surface chart for 1200 GMT, March 4, 1962.

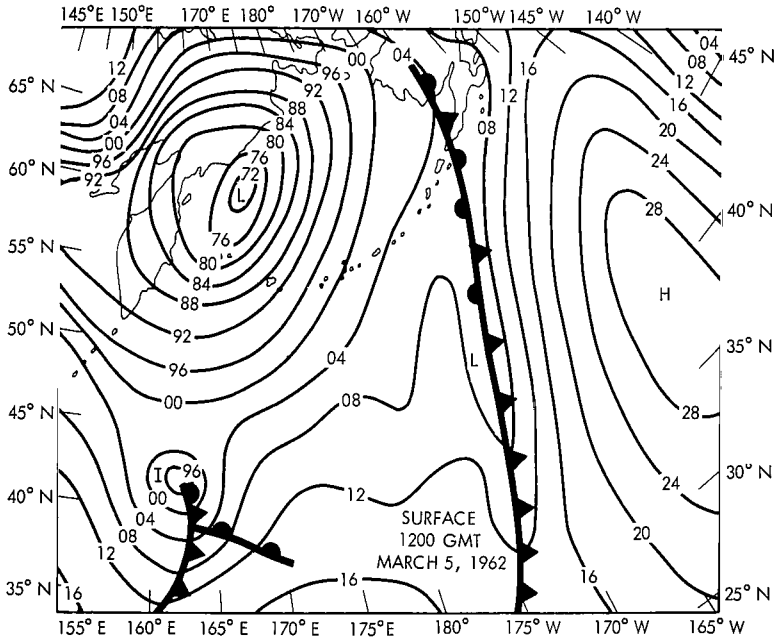

Figure 8—Surface chart for 1200 GMT, March 5, 1962.

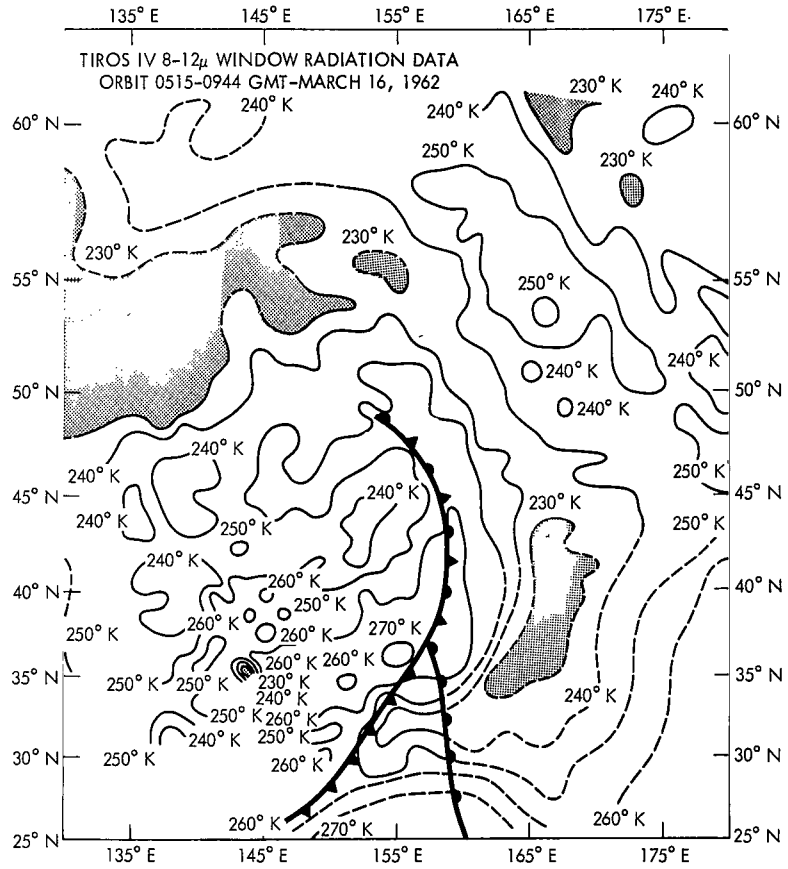

Figure 9—TIROS IV window radiation data for March 16, 1962 (orbit 515). Dashed lines show data added from orbits 514 and 516.

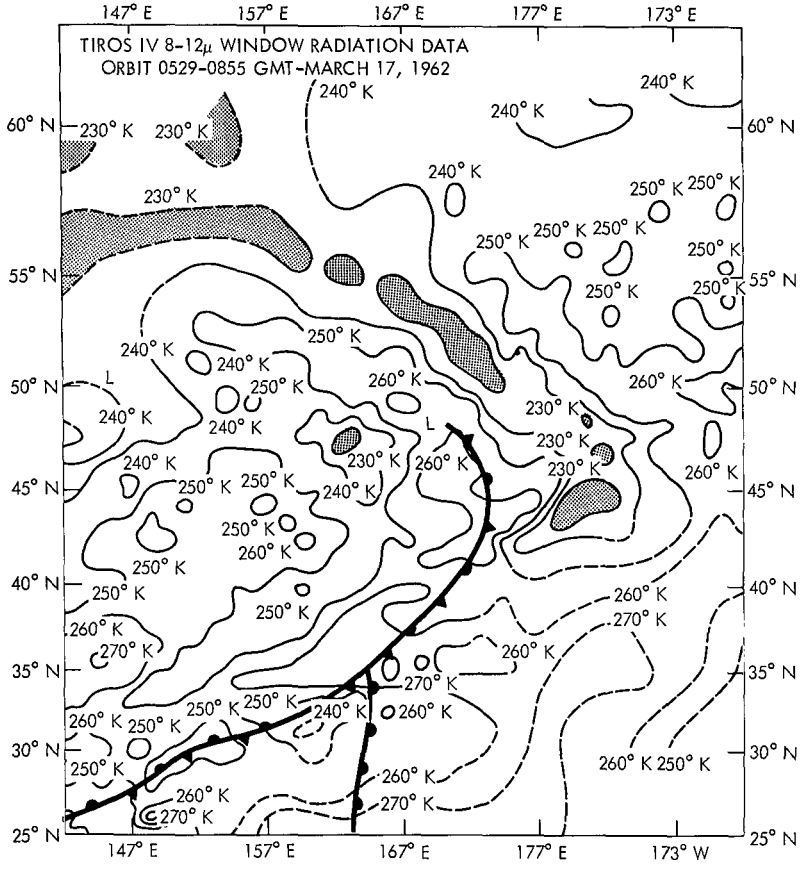

Figure 10—TIROS IV window radiation data for March 17, 1962 (orbit 529). Dashed lines show data added from orbits 528 and 530.

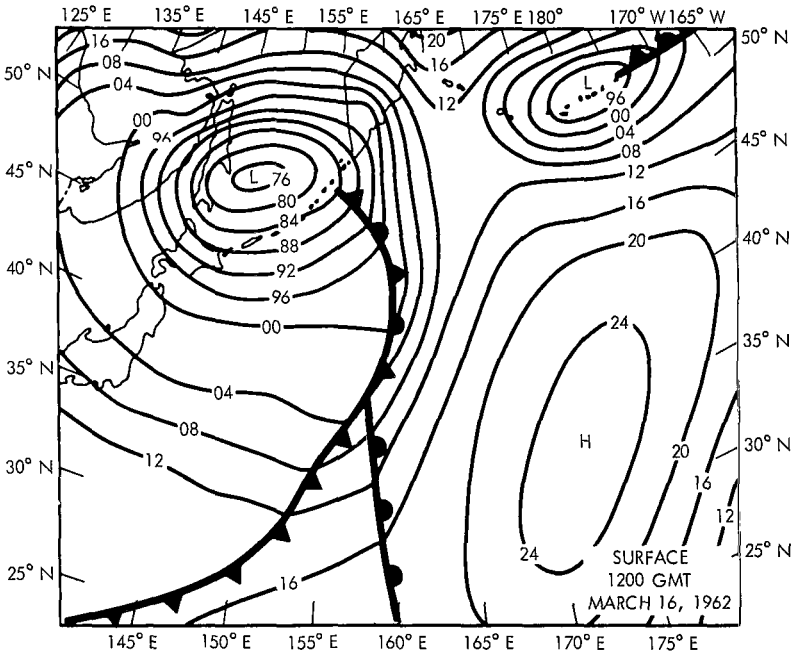

Figure 11—Surface chart for 1200 GMT, March 16, 1962.

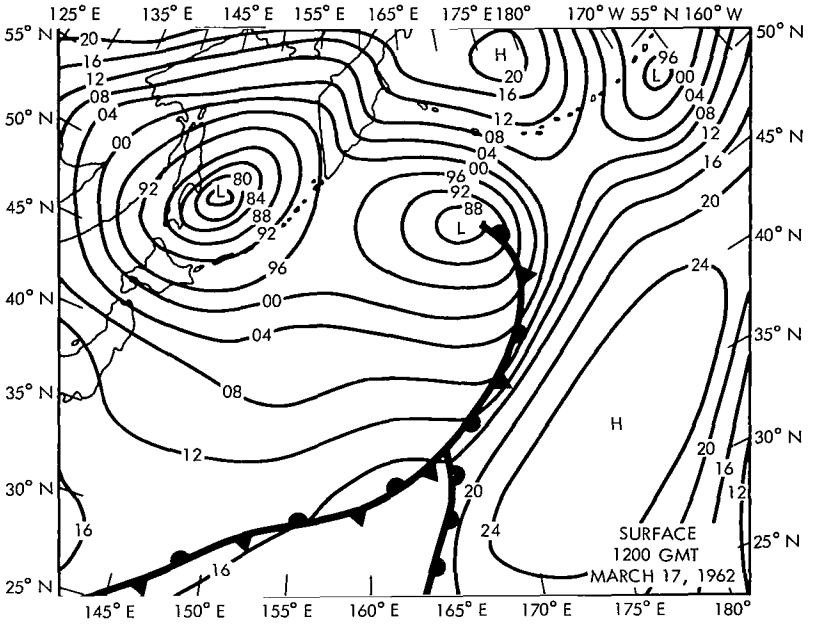

Figure 12—Surface chart for 1200 GMT, March 17, 1962.

area of high clouds either could have dissipated, or could have moved rapidly northeastward, closer to the region where a secondary cyclone did develop. In view of the upper level flow, it seemed most likely that the clouds dissipated.

The above mentioned secondary cyclone developed slowly between radiation map times well to the north of the base of the occlusion. Figure 11 shows the surface chart for 1200 GMT, March 16 where there is no evidence of a secondary circulation. First evidence of a new circulation was indicated on the 1800 GMT map for March 16 (chart not shown). No complete circulation was noticeable but the ship reports close to the new center suggested at least a weakness in the pressure gradient along the front. The evidence of a separate circulation center became stronger with each successive surface analysis (6 hour intervals) until at 1200 GMT, March 17 (Figure 12) the center was well defined. At 0900 GMT, March 17, the center of the new cyclone was located at 48°N, 170°E (Figure 10). The principal cloud band associated with the new storm is located to the east and north of the center. Equivalent blackbody temperatures of ≤ 230°K are present within this band, whereas 24 hours earlier there were no equivalent blackbody temperatures ≤ 230°K close to the region where the new system generated. Thus, the radiation data indicate that the cloud tops are probably higher in the same region relative to the new storm center after a new system is generated.

Figures 13-20 depict the window radiation grid print maps and surface weather charts that were coincident with a rapidly developing secondary cyclone in the eastern Pacific. The energetic new system developed suddenly near the base of the occlusion of an old and filling occluded cyclone of moderate intensity. The cloud top heights associated with the old primary cyclone were lower

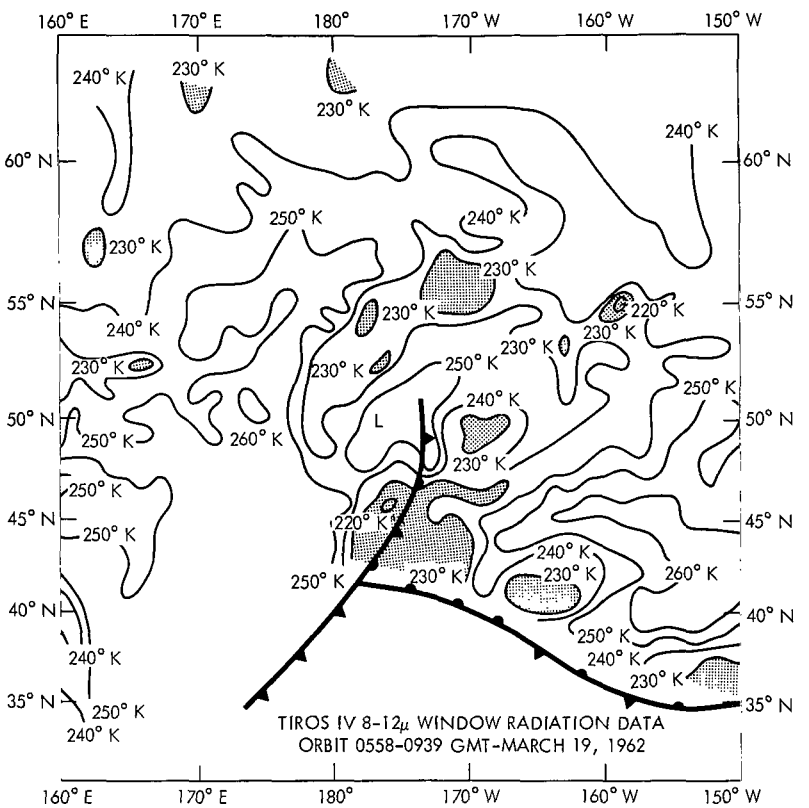

Figure 13—TIROS IV window radiation data for March 19, 1962 (orbit 558).

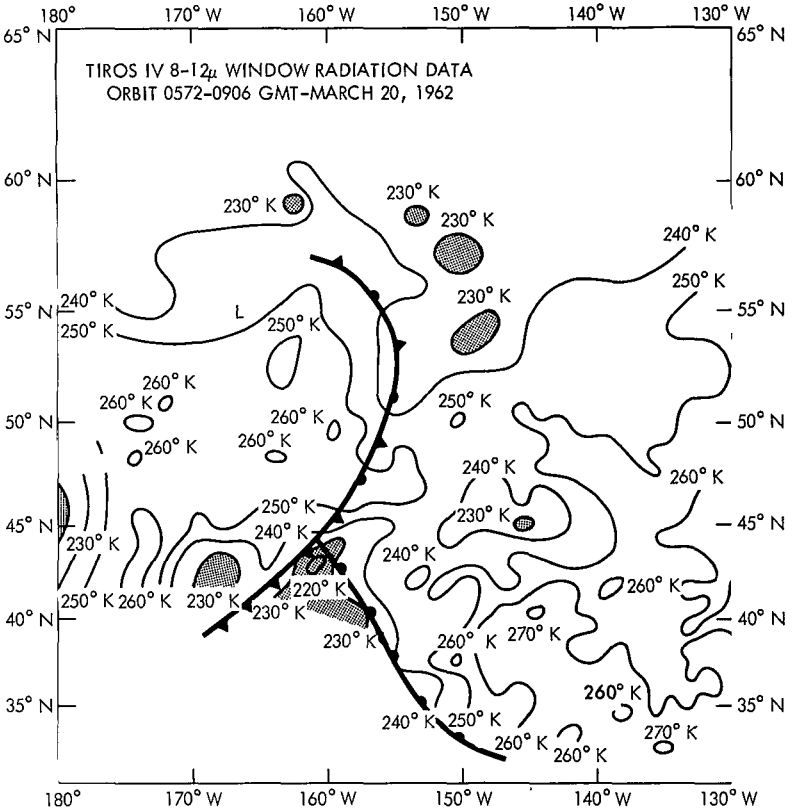

Figure 14—TIROS IV window radiation data for March 20, 1962 (orbit 572).

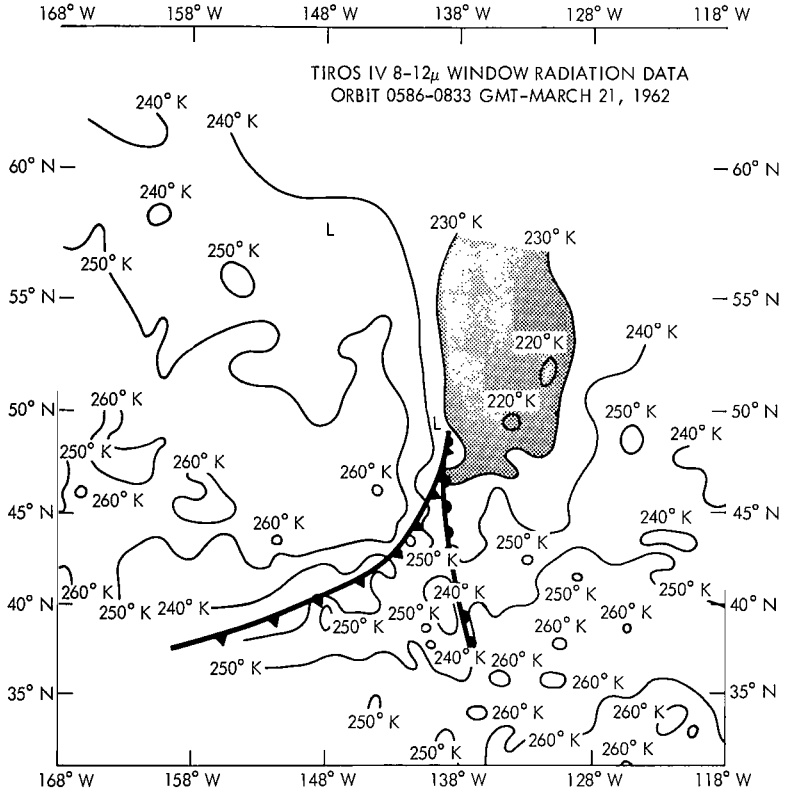

Figure 15—TIROS IV window radiation data for March 21, 1962 (orbit 586).

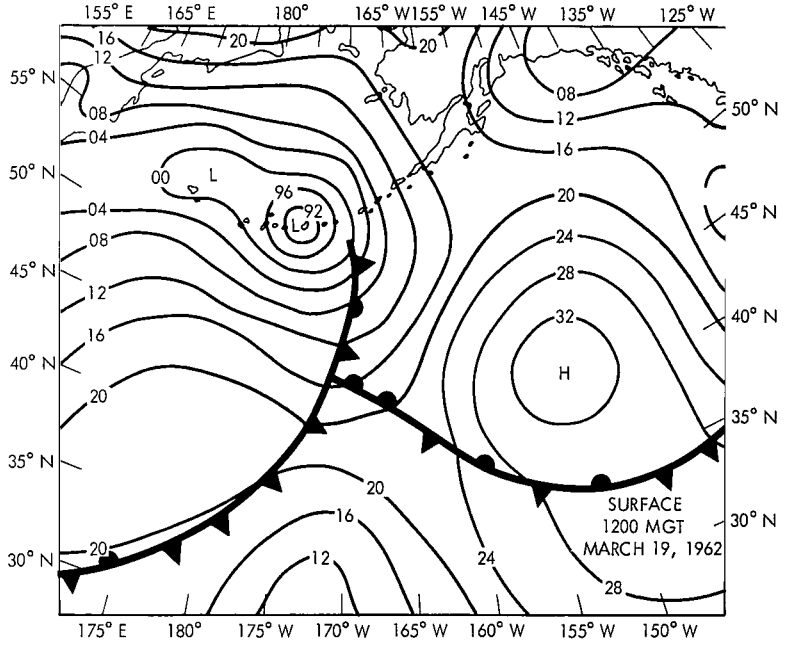

Figure 16—Surface chart for 1200 GMT, March 19, 1962.

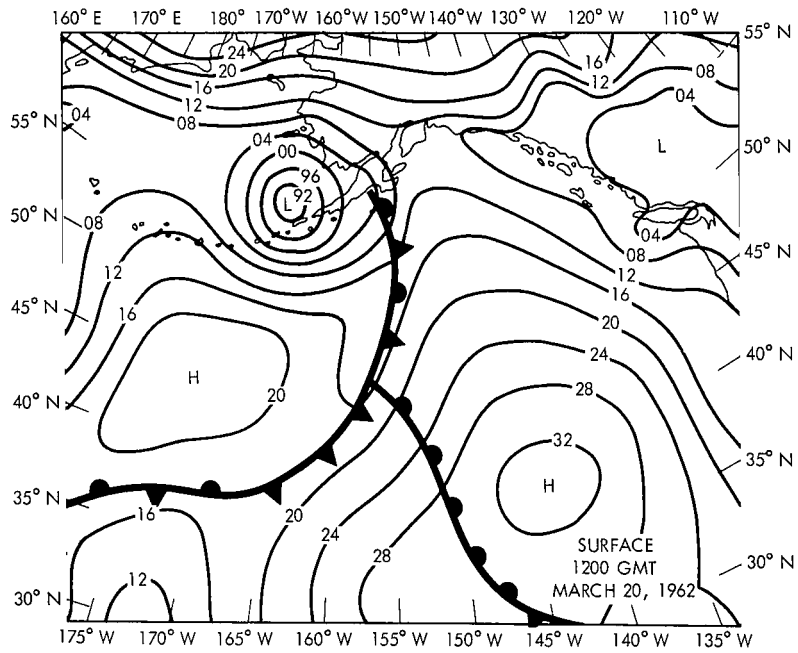

Figure 17—Surface chart for 1200 GMT, March 20, 1962.

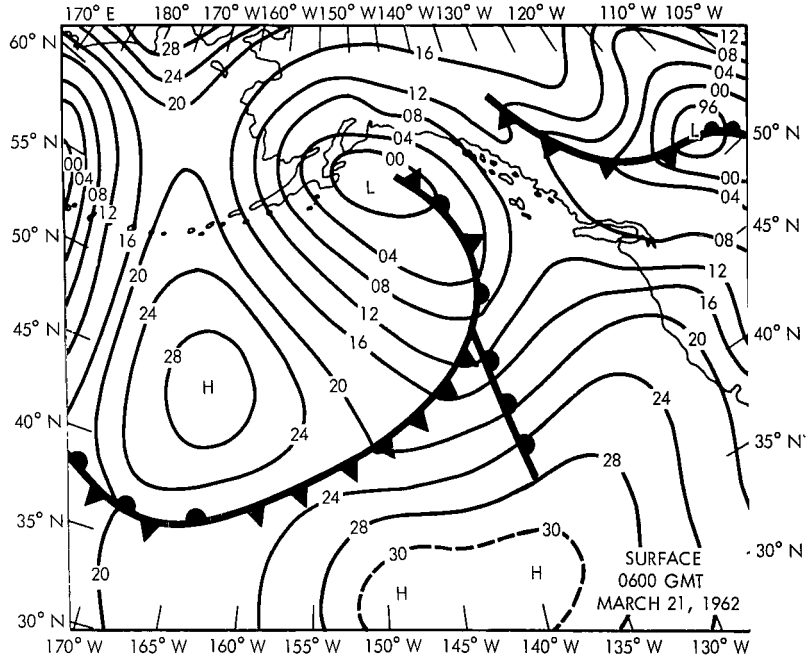

Figure 18—Surface chart for 0600 GMT, March 21, 1962.

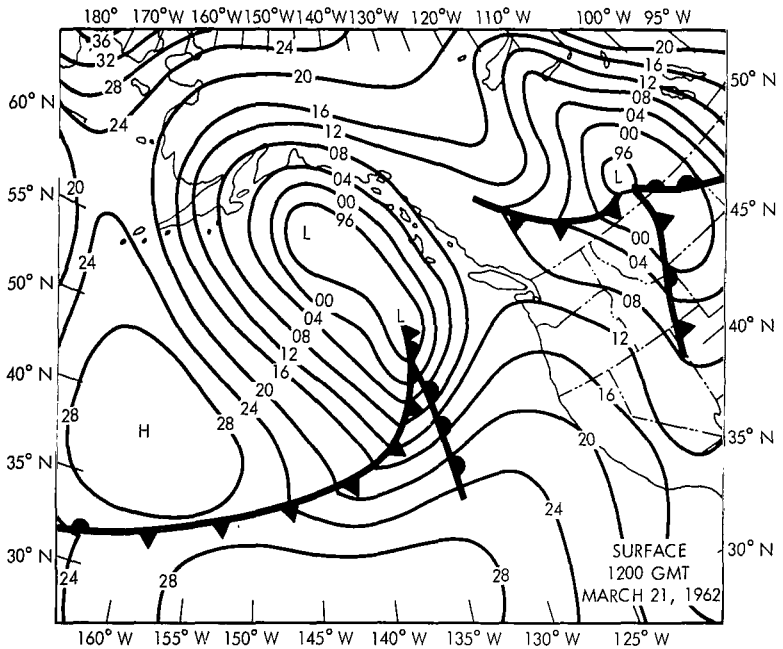

Figure 19—Surface chart for 1200 GMT, March 21, 1962.

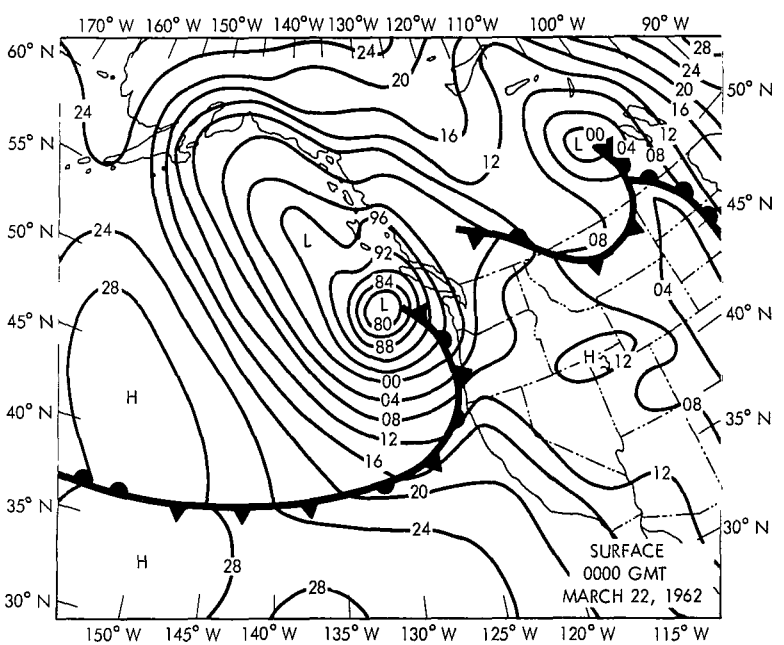

Figure 20—Surface chart for 0000 GMT, March 22, 1962.

(as measured by increased equivalent blackbody temperatures) in the region north and east of the base of the occlusion between 1000 GMT, March 19 and 0900 GMT, March 20 (Figures 13 and 14) although the central pressure of the storm did not change (Figures 16 and 17). The apparent decrease in cloud heights is shown by the almost total absence of equivalent blackbody temperatures $\leq 230\,^{\circ}K$ to the east and north of the base of the occlusion in Figure 14. In fact, some equivalent blackbody temperatures $\geq 250\,^{\circ}K$ occurred within that region. Thus, while it was not noticeable on the surface chart, the cloud pattern associated with the primary storm had undergone some deterioration. By 0600 GMT on March 21, the primary system had weakened and had continued to move steadily east-northeastward (Figure 18). There was no strong evidence of a secondary development in the surface analysis. The only possible hint was a 25kt west-northwest surface wind reported by a ship some 400 nautical miles south-southeast of the occluded cyclone center. This flow compares with a west to west-southwest flow of similar strength relative to the storm center some 18 hours earlier. The greater northerly component indicates that some low-level digging is starting to take place to the rear of the front. This evidence, although of interest, would almost certainly be insufficient to indicate an imminent surface development. A glance at the equivalent blackbody temperature field for 0900 GMT shows that sweeping changes had occurred in 24 hours (Figure 15). Instead of a rather disorganized cloud pattern east and north of the base of the occlusion, the equivalent blackbody temperature field indicates an area of solid high clouds over an extensive area. These high clouds probably reflect a dynamical trend towards stronger upward motions. Shenk (1963) showed that the strongest upward motions were associated with the lowest equivalent blackbody temperatures.

Tremendous changes began to occur on the surface charts within a few hours following the observation of the dramatic change in the cloud pattern. By 1200 GMT, March 21 (Figure 19) strong evidence was present that a new circulation was developing to the southeast of the old primary cyclone. Twelve hours later, the rapidly deepening and intensifying secondary cyclone was located not far from the West Coast of the United States and high winds were lashing the coastline (Figure 20). The new system deepened some 16 mb between 1200 GMT, March 21 and 0000 GMT, March 22. Thus, the strong trend towards lower equivalent blackbody temperatures between 0900 GMT, March 20 and 0900 GMT, March 21 had been coincident with a rapidly deepening secondary development.

A history similar to that observed on the surface charts occurred at 500 mb. Between 1200 GMT, March 19 and 0000 GMT, March 21, a short wave trough advanced through the central Pacific. It gradually weakened and was not detectable on the 0000 GMT, March 21 chart. Twelve hours later, a moderately strong, short wave trough was analyzed at about 140° - 150°W. Very strong cold advection on the upstream side of the trough line suggested continued digging and deepening of the trough. Thus, by 1200 GMT, March 21, it was evident from the analysis of the conventional data that a new cyclone was forming and that the potential existed for the development to continue. Undoubtedly, some cloud development had occurred before the TIROS pass (0900 GMT). This development, albeit perhaps less striking than what is shown, would have been useful in indicating the presence of favorable conditions for secondary development before it was reasonably certain that such development would occur from examining the available conventional data.

Another secondary cyclone developed one day later to the west of the strong eastern Pacific secondary. Figures 21-26 show the window radiation grid print maps and surface data except for a surface chart for 0600 GMT, March 21 (Figure 18). The window radiation chart for 0700 GMT, March 21 (Figure 21) illustrates the classical equivalent blackbody temperature pattern associated with a large strong ocean storm (Figure 22) with some suggestion of the "inverted fish hook" shape of the frontal cloud band. The highest clouds were located east of the surface center with equivalent blackbody temperatures of $\leq 220\,^{\circ}K$. Further south, to the east of the occluded front, the equivalent blackbody temperatures were mostly in the $230\,^{\circ}$-$240\,^{\circ}K$ range with small areas of equivalent blackbody temperatures of $\leq 230\,^{\circ}K$. Twenty-one hours (0400 GMT, March 22) later equivalent blackbody temperatures of $\leq 230\,^{\circ}K$ were more widespread in the area within 400 nautical miles to the north and east of the base of the occlusion, inferring a general increase in the cloud heights within that region (Figure 23).

There is no evidence of secondary development on the 0600 GMT, March 22 surface chart (Figure 24). Six hours later, a small circulation was analyzed east-southeast of the primary cyclone (Figure 25). No complete circulation was indicated from the ship data in the vicinity of the secondary, but the stretching of the isobars to the southeast of the filling primary cyclone appeared to justify the presence of a weak secondary circulation. By 0000 GMT, March 23 the presence of a complete circulation was confirmed by the ship data and by 0600 GMT, March 23 (Figure 26) the new cyclone was quite vigorous and had become the dominant circulation. Like the eastern secondary development described earlier, this cyclone produced considerable stormy weather on the West Coasts of Canada and the United States.

The above discussions suggest that, when a reversal occurs in the gradual increase of the equivalent blackbody temperatures associated with the weakening frontal cloud band of an existing cyclone, the probability of secondary cyclone development has increased. Figure 27 is a schematic drawing of an old occluded system and the dashed region represents one likely area where this reversal might occur. The temperature-reversal hypothesis was tested by computing the mean and frequency distributions of the equivalent blackbody temperatures within this dashed region for all four cases. This axis of the rectangle was always oriented north-south. As can be seen in Figure 27, the dashed area is determined by the position of the base of the occlusion which cannot always be located precisely over the oceans. However, this area is large and thus the precise location was not judged to be a critical factor. After the formation of a secondary cyclone, the lower left corner of the area was located at the secondary cyclone center. Table 2 presents the frequency distribution of equivalent blackbody temperatures within the dashed area, with class intervals of $10\,^{\circ}K$. The average equivalent blackbody temperatures were computed by assigning the values within each class to the central value of the class, except for the class of $\leq 220\,^{\circ}K$ where all values were assigned an equivalent blackbody temperature of $220\,^{\circ}K$. In the two cases where no substantial secondary development occurred at the base of the occlusion, a gradual day-to-day increase in the average equivalent blackbody temperature was noted within the dashed region. Also, there is a day-to-day decrease in the number of equivalent blackbody temperature measurements in the $221\,^{\circ} \leq 230\,^{\circ}K$ class. The average day-to-day increase in equivalent blackbody temperature within the dashed region was $4\,^{\circ}K$ when no substantial secondary development occurred.

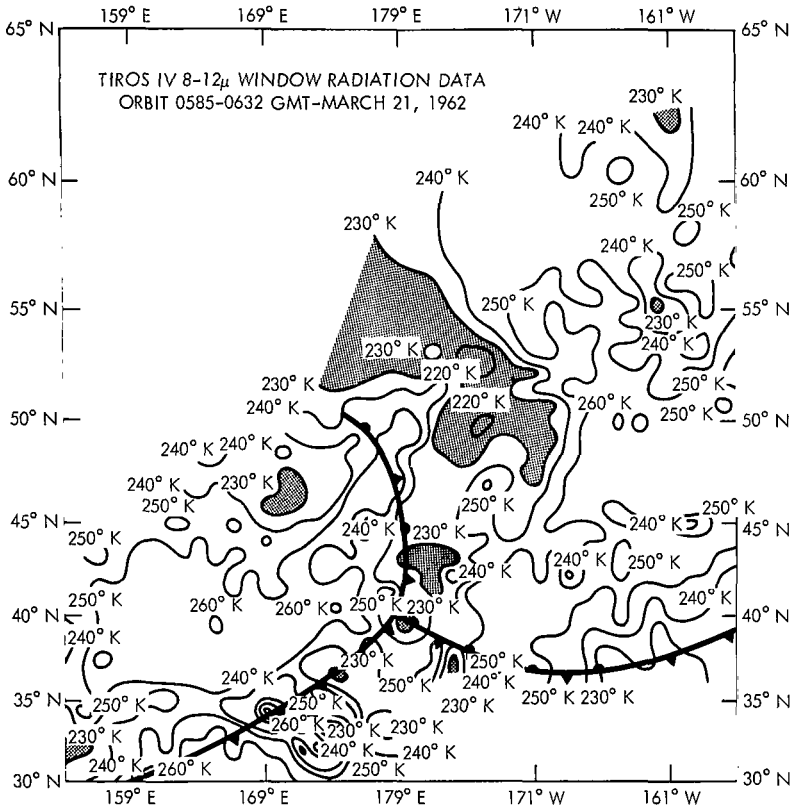

Figure 21—TIROS IV window radiation data for March 21, 1962 (orbit 585).

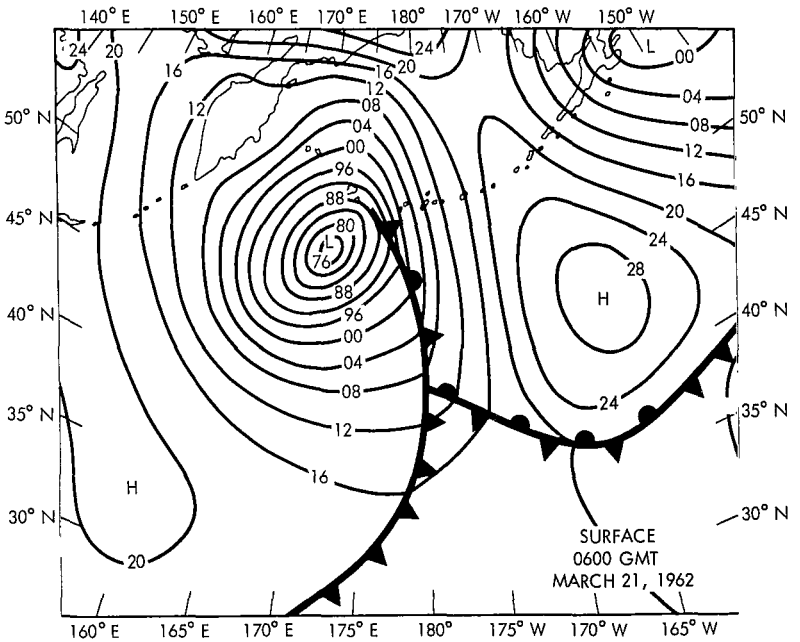

Figure 22—Surface chart for 0600 GMT, March 21, 1962.

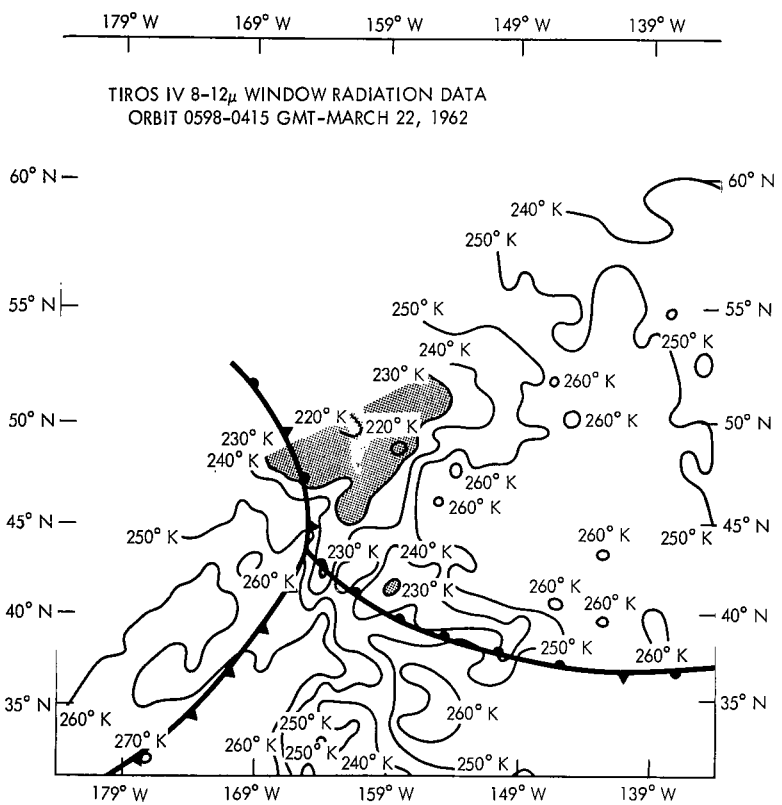

Figure 23—TIROS IV window radiation data for March 22, 1962 (orbit 598).

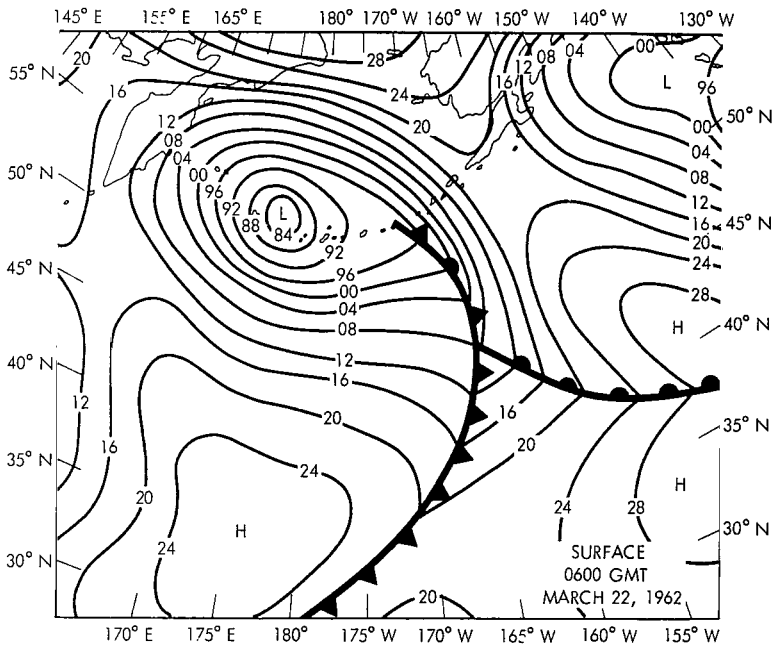

Figure 24—Surface chart for 0600 GMT, March 22, 1962.

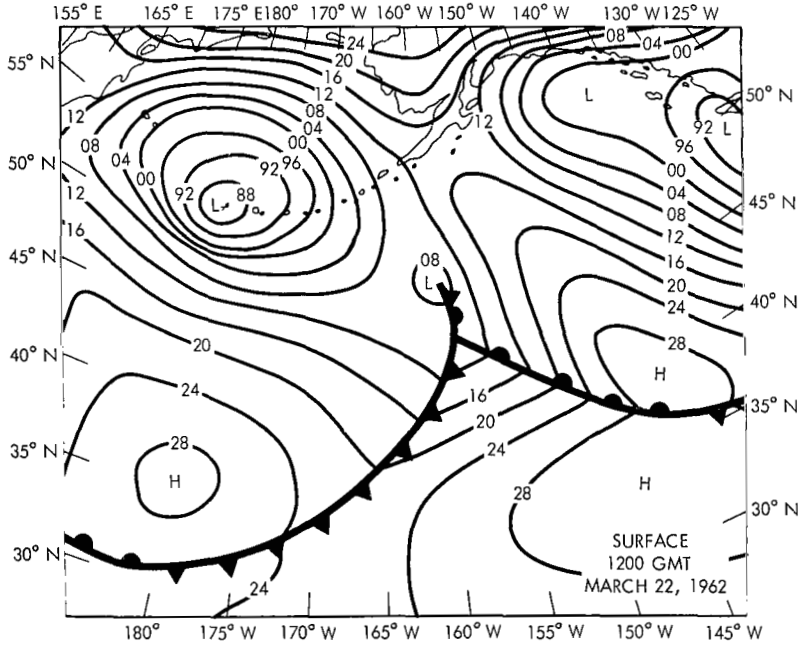

Figure 25—Surface chart for 1200 GMT, March 22, 1962

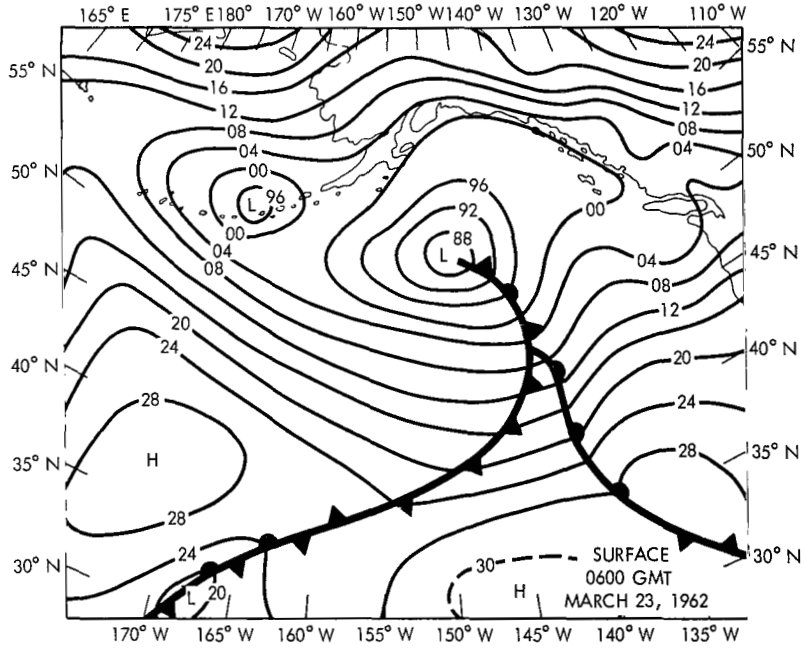

Figure 26—Surface chart for 0600 GMT, March 23, 1962.

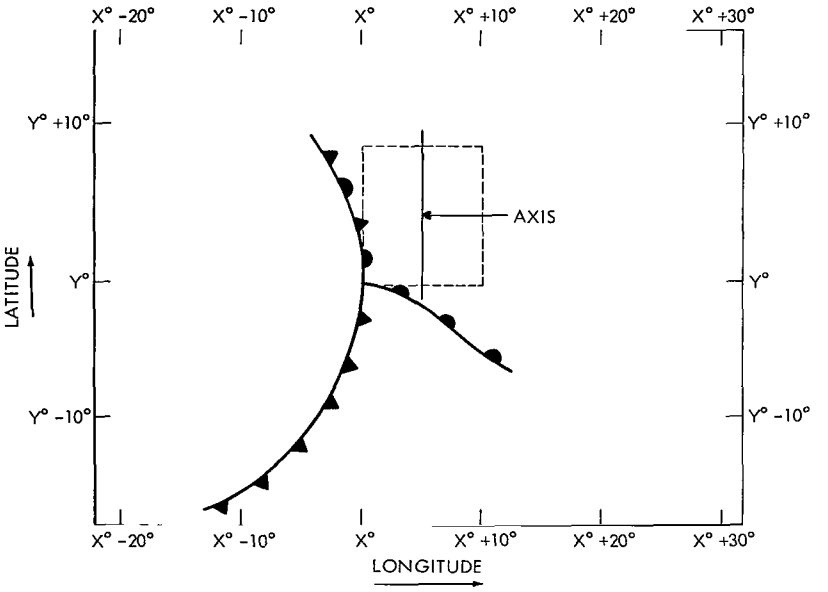

Figure 27—Schematic diagram of the frontal structure of an occluded cyclone. The dashed region is oriented north-south with the lower left corner at the triple point (latitude y°, longitude x°).

Table 2 shows that before the development of the March 21 secondary cyclone (case 3), there was a sharp rise (13.6°K) in the average equivalent blackbody temperature in the dashed area (1000 GMT, March 19 - 0900 GMT, March 20). This was followed by the even more dramatic decrease of 23.6°K in equivalent blackbody temperature in the next period. Figure 28 illustrates the frequency distributions for the equivalent blackbody temperature within the dashed region for the three window radiation grid print maps associated with this case. The sharp frequency shifts of the 221° $\leq$ 230°K class are readily apparent. The decrease in equivalent blackbody temperatures within the dashed region also occurred with the other case of secondary development, although the equivalent blackbody temperature decrease was less (6.5°K). Therefore, when secondary cyclone generation was noted, the average equivalent blackbody temperature decrease was 15°K.

CONCLUSIONS

These four case studies indicate that when a secondary cyclone is beginning to form at the surface near the base of the occlusion, a substantial day-to-day decrease in the equivalent blackbody temperature has already occurred in an area within a few hundred miles to the northeast of the center of the new circulation. No equivalent blackbody temperature decrease was noted within the same area when no new development or a very weak stable wave developed. The equivalent blackbody temperature decrease was greatest for the case where the secondary cyclone developed

Table 2

Frequency of TIROS IV Window Radiation Measurements Within 10K Class Limits for Each Case Within the Dashed Region Shown in Figure 27.

Equivalent Blackbody Temperatures (°K)	Date and Principal Orbit Number		
	Case 1		
	March 3, 1962 (330)	March 4, 1962 (344)	March 5, 1962 (358)
220	0	0	0
221 ≤ 230	42	37	13
231 ≤ 240	18	24	47
241 ≤ 250	6	8	10
251 ≤ 260	6	3	2
Average	231.7°K	231.8°K	235.1°K
	Case 2		
	March 16, 1962 (515)		March 17, 1962 (529)
220	0		0
221 ≤ 230	10		0
231 ≤ 240	10		0
241 ≤ 250	15		6
251 ≤ 260	20		40
261 ≤ 270	17		24
271 ≤ 280	0		2
Average	248.3°K		258.1°K
	Case 3		
	March 19, 1962 (558)	March 20, 1962 (572)	March 21, 1962 (586)
220	1	0	2
221 ≤ 230	36	0	58
231 ≤ 240	18	9	12
241 ≤ 250	7	39	0
251 ≤ 260	10	24	0
Average	233.5°K	247.1°K	223.5°K
	Case 4		
	March 21, 1962 (585)		March 22, 1962 (598)
220	0		1
221 ≤ 230	8		33
231 ≤ 240	36		14
241 ≤ 250	16		9
251 ≤ 260	12		6
Average	239.4°K		232.9°K

most rapidly. This result suggests that the rapidity of surface development may be related to the rate of change of equivalent blackbody temperature within the frontal cloud band.

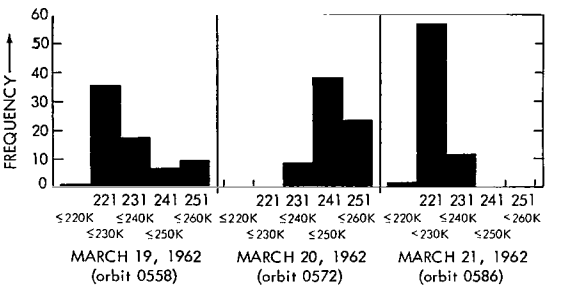

Figure 28—Frequency distributions for three orbits (558, 572, 586) of equivalent blackbody temperatures within the dashed rectangle shown in Figure 27.

The onset of cloud development relative to surface development should be examined more closely. This might be possible with the receipt of infrared measurements in the fall, winter, or spring seasons at twelve-hour intervals from a polar orbiting satellite. Even better cloud-surface development relationships should be possible as soon as radiometers are placed in geosynchronous orbit when observations will be made at intervals of less than an hour. In addition to better temporal resolution, current or planned sensors placed in these orbits will have better thermal and spatial resolutions than were possible with the earlier satellites. The improved resolutions should afford a better definition of the cloud surfaces and hence, permit a deeper probing into this type of meteorological phenomena.

Goddard Space Flight Center
National Aeronautics and Space Administration
Greenbelt, Maryland, October 7, 1969
160-44-03-02-51

REFERENCES

1. Anderson, R. K., Ferguson, E. W., and Oliver, V. J., "The Use of Satellite Pictures in Weather Analysis and Forecasting," World Meteorological Organization Technical Note No. 75, Geneva, Switzerland, 1966.

2. Boucher, R. J., Bowley, C. J., Merritt, E. S., Rogers, C. W. C., Sherr, P. E., and Widger, W. K., Jr., "Synoptic Interpretations of Cloud Vortex Patterns as Observed by Meteorological Satellites," Aracon Geophysics Co., Concord, Mass., Final Report, Cwb-10630. Prepared for U. S. Weather Bureau, National Weather Satellite Center, November 1963.

3. Sherr, P. E., and Rogers, C. W. C., "The Identification and Interpretation of Cloud Vortices Using TIROS Infrared Observation," Aracon Geophysics Co., Concord, Mass., Final Report, Cwb-10812. Prepared for U. S. Weather Bureau, National Weather Satellite Center, March 1965.

4. TIROS IV Radiation Data Catalog and Users' Manual, NASA, Goddard Space Flight Center, Aeronomy and Meteorology Division, Greenbelt, Maryland, December 15, 1963.

5. Bandeen, W. R., "TIROS II Radiation Data User's Manual Supplement," Aeronomy and Meteorology Division, Goddard Space Flight Center, Greenbelt, Maryland, May 15, 1962.

6. Shenk, W. E., "TIROS II Window Radiation and Large Scale Vertical Motion," *J. Applied Meteorology*, 2(6):770-775, December 1963.

NASA-Langley, 1970 —— 20

NATIONAL AERONAUTICS AND SPACE ADMINISTRATION
WASHINGTON, D. C. 20546

OFFICIAL BUSINESS

FIRST CLASS MAIL

POSTAGE AND FEES PAID
NATIONAL AERONAUTICS AND
SPACE ADMINISTRATION

"The aeronautical and space activities of the United States shall be conducted so as to contribute . . . to the expansion of human knowledge of phenomena in the atmosphere and space. The Administration shall provide for the widest practicable and appropriate dissemination of information concerning its activities and the results thereof."

—NATIONAL AERONAUTICS AND SPACE ACT OF 1958

NASA SCIENTIFIC AND TECHNICAL PUBLICATIONS

TECHNICAL REPORTS: Scientific and technical information considered important, complete, and a lasting contribution to existing knowledge.

TECHNICAL NOTES: Information less broad in scope but nevertheless of importance as a contribution to existing knowledge.

TECHNICAL MEMORANDUMS: Information receiving limited distribution because of preliminary data, security classification, or other reasons.

CONTRACTOR REPORTS: Scientific and technical information generated under a NASA contract or grant and considered an important contribution to existing knowledge.

TECHNICAL TRANSLATIONS: Information published in a foreign language considered to merit NASA distribution in English.

SPECIAL PUBLICATIONS: Information derived from or of value to NASA activities. Publications include conference proceedings, monographs, data compilations, handbooks, sourcebooks, and special bibliographies.

TECHNOLOGY UTILIZATION PUBLICATIONS: Information on technology used by NASA that may be of particular interest in commercial and other non-aerospace applications. Publications include Tech Briefs, Technology Utilization Reports and Notes, and Technology Surveys.

Details on the availability of these publications may be obtained from:

SCIENTIFIC AND TECHNICAL INFORMATION DIVISION

NATIONAL AERONAUTICS AND SPACE ADMINISTRATION

Washington, D.C. 20546